RMetS

Royal Meteorological Society

Climate sensitivity of Mediterranean pine growth reveals distinct east–west dipole

Andrea Seim,[a,*] Kerstin Treydte,[b] Valerie Trouet,[c] David Frank,[b,d] Patrick Fonti,[b]
Willy Tegel,[e] Momchil Panayotov,[f] Laura Fernández-Donado,[g,h] Paul Krusic[i] and Ulf Büntgen[b,d,j]

[a] *Regional Climate Group, Department of Earth Sciences, University of Gothenburg, Sweden*
[b] *Swiss Federal Research Institute WSL, Birmensdorf, Switzerland*
[c] *Laboratory of Tree-Ring Research, University of Arizona, Tucson, AZ, USA*
[d] *Oeschger Centre for Climate Change Research, Bern, Switzerland*
[e] *Institute of Forest Sciences, University of Freiburg, Germany*
[f] *Dendrology Department, University of Forestry, Sofia, Bulgaria*
[g] *Departamento de Astrofísica y Ciencias de la Atmósfera, Facultad de Ciencias Físicas, Universidad Complutense de Madrid, Spain*
[h] *Facultad de CC. Fisicas, Instituto de Geociencias (CSIC-UCM), Madrid, Spain*
[i] *Physical Geography and Quaternary Geology, Stockholm University, Stockholm and Navarino Environmental Observatory, Messinia, Greece*
[j] *Global Change Research Centre AS CR, Brno, Czech Republic*

ABSTRACT: The European Mediterranean region is governed by a characteristic climate of summer drought that is likely to increase in duration and intensity under predicted climate change. However, large-scale network analyses investigating spatial aspects of pre-instrumental drought variability for this biogeographic zone are still scarce. In this study we introduce 54 mid- to high-elevation tree-ring width (TRW) chronologies comprising 2186 individual series from pine trees (*Pinus* spp.). This compilation spans a 4000-km east–west transect from Spain to Turkey, and was subjected to quality control and standardization prior to the development of site chronologies. A principal component analysis (PCA) was applied to identify spatial growth patterns during the network's common period 1862–1976, and new composite TRW chronologies were developed and investigated. The PCA reveals a common variance of 19.7% over the 54 Mediterranean pine chronologies. More interestingly, a dipole pattern in growth variability is found between the western (15% explained variance) and eastern (9.6%) sites, persisting back to 1330 AD. Pine growth on the Iberian Peninsula and Italy favours warm early growing seasons, but summer drought is most critical for ring width formation in the eastern Mediterranean region. Synoptic climate dynamics that have been in operation for the last seven centuries have been identified as the driving mechanism of a distinct east–west dipole in the growth variability of Mediterranean pines.

KEY WORDS   climate dynamics; dendroclimatology; drought response; Mediterranean east-west dipole; palaeoclimatology; *Pinus* spp; principal component analysis; tree-ring width

Received 11 May 2014; Revised 27 June 2014; Accepted 23 July 2014

1. Introduction

The European Mediterranean region represents a unique climatic zone where drought-prone ecosystems have developed under strong environmental constraints including perpetual summer drying and extensive settlement pressure. Projected global warming will probably have an impact on the hydrological cycle in this region (IPCC, 2013). General circulation models forecast a decrease in precipitation and increase in temperature, together with an increase in the frequency and severity of weather extremes such as floods and heat waves (Gao and Giorgi, 2008). To facilitate accurate future climate scenarios and related ecological implications for this region, quantitative information about pre-industrial climate conditions, derived from proxy climate records, is needed.

Predicting future climate scenarios for the Mediterranean region is challenging because climatic fluctuations exhibit a high degree of spatial variability due to the complex interaction of synoptic modes (Dünkeloh and Jacobeit, 2003). This complexity is mainly governed by meridional climatic differences representing the transition from the temperate zone in the north to the subtropics in the south. The land–sea distribution and significant orographic features also influence local climatic conditions. Numerous investigations based on instrumental climate and re-analyses data, especially for the winter season, have provided an improved understanding of regional climate differences in the Mediterranean Basin. However, these studies are largely restricted to the last 50 years (e.g. Xoplaki *et al.*, 2003; Sousa *et al.*, 2011) and only a limited number of annually resolved climate proxy data is
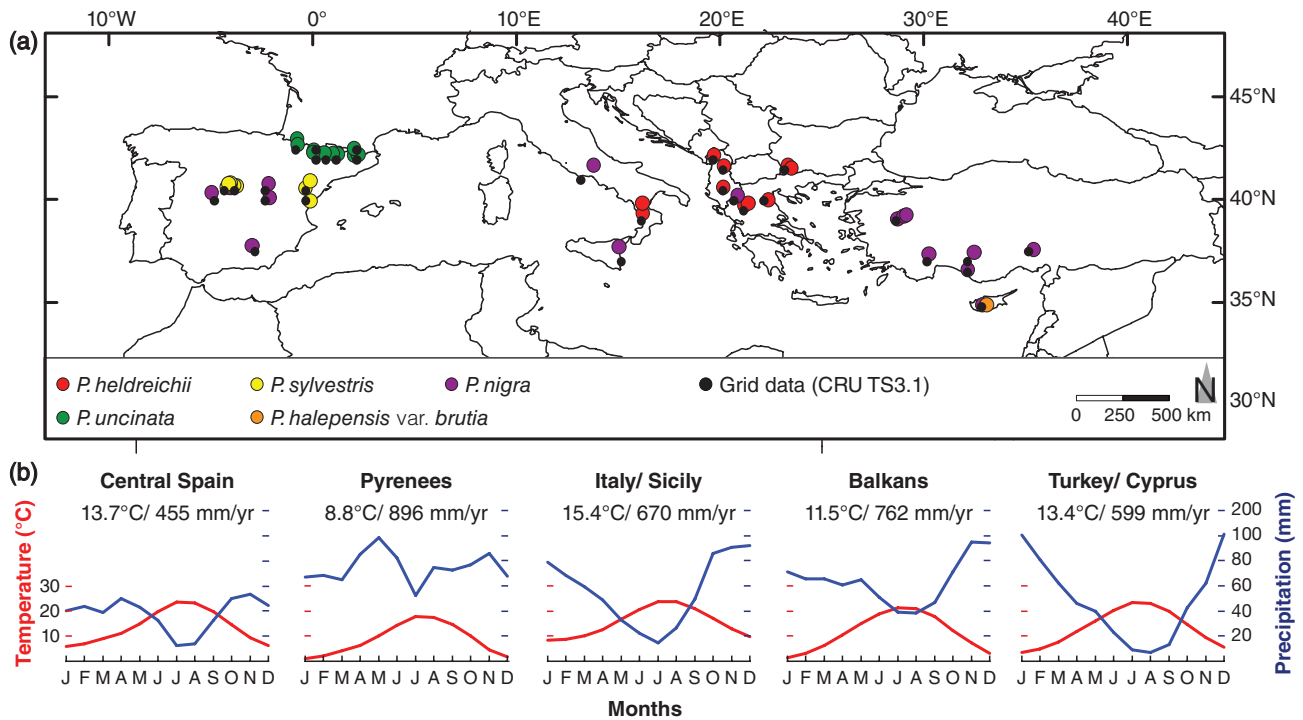
Figure 1. (a) Mediterranean TRW network of 54 pine sites and their closest grid points (CRU TS3.1). (b) Seasonal temperature and precipitation (red and blue lines) variability averaged over the period 1961–1990 and obtained from the CRU TS3.1 data corresponding to the five main TRW network regions.

available to extend this record further back in time (refer Luterbacher *et al.*, 2012 for a review).

Tree-ring width (TRW) chronologies, the most prevalent of these proxy data, are characterized by a broad spatial distribution, and provide temporal coverage over most of the last millennium at annual resolution. The pine genus (*Pinus* spp.) is a native, long-lived, ubiquitous component of Mediterranean flora (Barbéro *et al.*, 1998) enabling the development of well-replicated and dense networks over large spatial and long temporal scales. Pine trees are of particular interest because they exhibit a large ecological amplitude and various adaptation strategies, and form natural forest stands up to the timber line in the Mediterranean Basin. So far, the majority of conducted dendroclimatological studies using Mediterranean trees have largely been restricted to local scales (e.g. Büntgen *et al.*, 2010a; Seim *et al.*, 2012), occasionally to subregional scales (e.g. Richter *et al.*, 1991; Hughes *et al.*, 2001; Touchan *et al.*, 2014), or to one single species at large scale (de Luis *et al.*, 2013). The only spatial field reconstruction for the Mediterranean was developed by Nicault *et al.* (2008) and addresses summer drought variability in a multi-species network over the past 500 years.

Here, we evaluate the growth–climate response of a substantial collection of 54 pine TRW site chronologies from mid- to high elevations in the Mediterranean Basin. Regional-scale growth patterns were identified using principal component analysis (PCA) for the common period 1862–1976. New composite TRW chronologies were developed for three main and five subregions that were compared, assessed, and discussed with respect to possible causes for regional pine growth variability, prevailing synoptic climate forcing, and the potential for future drought reconstructions.

2. Data and methods

2.1. Network establishment

We compiled a network of 2186 TRW series from 54 pine sites across the Mediterranean region (Figure 1 and Table S1, Supporting Information). Only raw chronologies spanning more than 200 years, with an inter-series correlation (Rbar) above 0.45, were considered (Table S1). In total, 13 TRW chronologies were contributed by the authors, 39 TRW chronologies were selected from the International Tree-Ring Data Bank (ITRDB, http://www.ncdc.noaa.gov/paleo/treering.html; Grissino-Mayer and Fritts, 1997), and two chronologies, one from Greece and one from Italy, were kindly provided by P.I. Kuniholm and L. Todaro, respectively. The genus composition in this pine network includes *P. halepensis* var. *brutia* Hen., *P. heldreichii* Christ plus *P. heldreichii* var. *leucodermis* Ant., *P. nigra* Arn., *P. sylvestris* L., and *P. mugo* spp. *uncinata* (Ramond) Domin.

Cross-dating of all TRW series was first visually checked and then statistically verified using the program COFECHA (Holmes, 1983). To preserve growth variation on inter-annual to multi-decadal timescales, age-related growth trends were removed from all individual TRW series using 150-year cubic smoothing splines (150 year SPL) after power transformation (PT) (Cook and Peters, 1997), via the application of the program ARSTAN

(Cook and Krusic, 2010). TRW chronologies were truncated at a minimum of five series. The robustness of the chronologies was evaluated by the expressed population signal (EPS; Wigley *et al.*, 1984) that was calculated over 50-year periods with 25 years of overlap.

2.2. Instrumental data

A high-resolution ($0.5° \times 0.5°$) monthly resolved dataset of gridded climate indices (CRU TS3.1; Mitchell and Jones, 2005) was used to assess the climate sensitivity of the individual site chronologies. Temperature, precipitation, and drought (self-calibrated Palmer Drought Severity Index (scPDSI); van der Schrier et al., 2006) anomalies, with respect to their 1961–1990 averages, were calculated for the period 1901–2002 for each grid point closest to the TRW sites (Figure 1(a)). In a next step, the climate variables from individual grid points were averaged in correspondence with the outcome of the PCA (Section 2.3). In the correlation analysis, we used 31 grid boxes of temperature and precipitation data, and 30 grid boxes of scPDSI data because the latter were only available north of 35°N. The grand means of all Rbar values of annual temperature, precipitation, and scPDSI data across the network are 0.57 ($p < 0.001$), 0.21 ($p < 0.05$), and 0.26 ($p < 0.05$), respectively, indicating comparable temperature but heterogeneous moisture conditions across the region. Pearson's correlation coefficients were calculated between TRW records and means of monthly temperature, scPDSI, and sums of monthly precipitation, using an 18-month window from previous year's May to current October. Spatial correlations with CRU TS3.1 data were calculated and plotted using the KNMI Climate Explorer (http://climexp.knmi.nl; van Oldenborgh and Burgers, 2005; Trouet and van Oldenborgh, 2013).

2.3. Spatial analyses

We applied a PCA (Peters *et al.*, 1981) including all 54 TRW site chronologies in order to identify systematic growth patterns inherent to the pine network over the 1862–1976 common period. All principal components (PCs) with eigenvalues greater than 1 were retained for further analysis. The first PC was used to determine the primary climatic driver of common variance and loadings along the second and third PC axes served as the basis for regional subdivision resulting in three main groups. This procedure was repeated using chronologies categorized by PC2 and PC3, which resulted in five additional subgroups (all labelled with respect to the PCA outcome as shown in Figure 3(a)). Composite chronologies were developed for the eight network groupings by averaging the individual TRW series of all sites in a group. Hierarchical cluster analysis (Ludwig and Reynolds, 1988) over the same common period was conducted to verify the PCA outcome (Figure S1).

Potential differences and similarities in the temporal variability of the two main groups were investigated on the basis of 20-year high- and low-pass filtered composite TRW records. Additionally, extreme years were defined as years when the absolute value of the high-pass filtered TRW records exceeded the 1.5 standard deviation.

To evaluate the spatial decay in intra- and inter-species signal strength, correlations were computed as a function of distance between all sites in the network (54 TRW and 31 climatic grid points) for the periods 1862–1976 (TRW) and 1901–1976 (climate). The same approach was used for temperature and precipitation grid-point data for winter (previous year December to current year February, DJF) and summer (June to August, JJA).

Finally, factors influencing tree growth were analysed using cross correlations including climatic and geographic aspects, as well as species and site chronology characteristics.

3. Results

3.1. Network characteristics and regionalization

The maximum and minimum length of the chronologies after truncation $n(i) < 5$ series is 1041 years (968–2008; Lura, Albania) and 142 years (1862–2003; Scotida Forest, Greece) (Figure 2 and Table S1). The mean
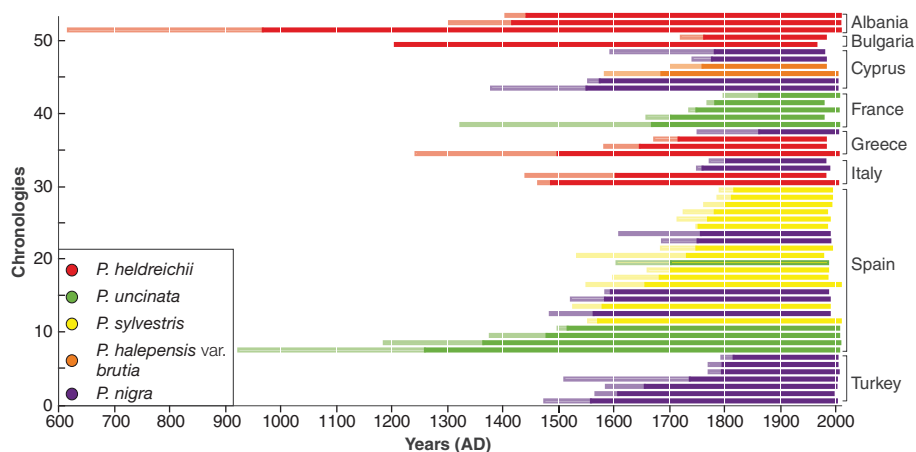

Figure 2. Replication of the TRW network by country, in alphabetical order, and record lengths. Each bar represents one individual chronology and colors represent different pine species. Colors refer to chronologies' length after truncation $n(i) < 5$ series, whereas shadings denote their full lengths.
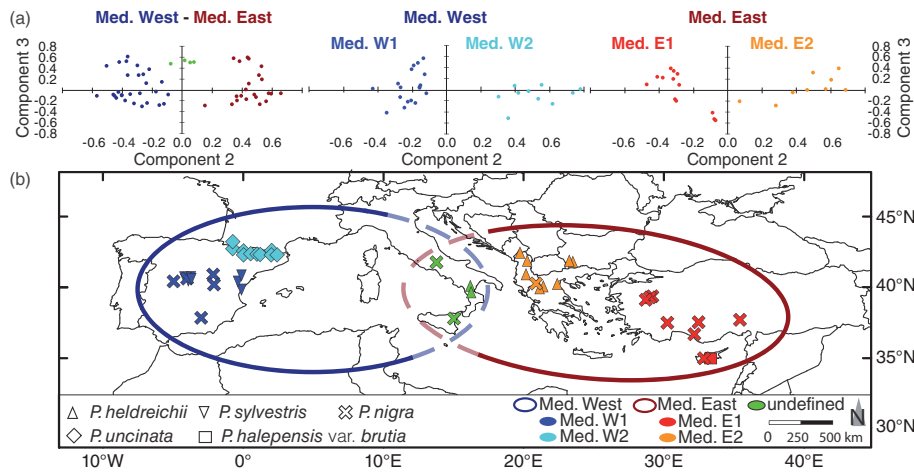
Figure 3. (a) Scatter plots of the PCA of all sites (power transformed 150-year spline detrended TRWchronologies) indicating the main PCs Med. West and Med. East and their subgroups (Med. W 1, Med. W2 and Med. E1, Med. E2) for the common period 1862–1976. (b) Spatial distribution of the various PCs (main PCs as ellipse, subgroups in graduated colors) relative to tree species (symbols).

segment length (MSL) of all chronologies is 345 years after truncation. The number of samples per site varies from 11 (Troodos Mountain, Cyprus) to 200 (Gerber, Spain) with a mean of 41 (Table S1). The first six PCs (eigenvalue > 1) of the entire network explain 62% of the total common variance (Figure 3). Similar results were obtained for the pre-whitened residuals (not shown), but we used standardized residuals throughout the experiment. The first PC alone (herein referred to as Med.) explains 19.7% of the common variance over the entire pine network. The network can be divided into three geographically distinct regions based on PC2 (representing 15% of the total variance): sites in the western Mediterranean region (Med. West) have negative loadings on PC2 (-0.57 to -0.09; Figure 3), whereas sites in the eastern Mediterranean region (Med. East) have positive loadings ($0.15-0.66$). Sites in Italy have PC2 loadings close to zero (-0.08 to 0.08) and thus form a third geographical group.

The Med. West group consists of 32 site chronologies. The first three axes of these 32 chronologies cumulatively explain 51.5% of their total variance. The first axis explains 29.5% of the common variance, and all series have positive scores ranging from 0.3 (Pic d'Anie, France) to 0.8 (Guadarrama, Loma de Noruego, Spain). The Med. West group can be subdivided based on PC2 (13.7%) representing chronologies from central Spain (Med. W1, 18 chronologies) and the Pyrenees (Med. W2, 10 chronologies; Figure 3).

The first three PCs of the Med. East (22 chronologies) explain a slightly higher amount of total common variance (63.6%) with the first axis explaining 39.7% common variance with positive loading scores ranging from 0.4 (Kozlu Pinari, Turkey) to 0.8 (Kirazli, Aligalani, Atalani, Turkey). Based on PC2 (15.8% common variance), two subgroups can be distinguished: Turkey and Cyprus (Med. E1) and the Southern Balkans (Med. E2).

Based on the PC analyses, regional composite TRW chronologies were developed by aggregating the corresponding individual TRW series. All relevant statistics for

the three regional groups and the five regional subgroups are shown in Table 1. Hierarchical cluster analysis revealed similar results by splitting the TRW network in five subgroups including an individual Italian group (Figure S1).

The temporal coherency analysis between the detrended composite TRW chronologies Med. West and Med. East revealed limited common variability ($r = 0.1$, $p > 0.1$) over the well-replicated ($n > 800$ series) and robust period 1330–2008 (Figure 4(a) and (b)). This low coherence is confirmed in both the low- and high-frequency domains over three 338/339-year-long correlation periods (1330–1669, 1500–1838, and 1669–2008) (Figure 4).

Moreover, of 42/46 positive/negative extreme years for West and 55/46 positive/negative extremes for East, only nine positive (1411, 1452, 1499, 1541, 1590, 1846, 1885, 1914, and 1959) and five negative (1602, 1725, 1806, 1880, and 1909) extreme years are in common. An association between the extreme years calculated for the West and East group is not significant at the 95% confidence level ($p = 0.384$). The 14 common extreme years are also extremes in the Med. chronology (PC1). From the total of 49/50 positive/negative extreme years for this chronology, 10/12 positive/negative extreme years are unique for the Mediterranean as a whole.

3.2. Spatial characteristics

Correlations of the 54 TRW chronologies as a function of species and distance, for the common period 1862–1976, are shown in Figure S2. The total number of pairs used in the intra-species curve is 583 and, in the inter-species, is 2239.

The highest positive intra-species correlation is $r = 0.58$ ($p < 0.001$) for neighbouring sites, i.e. 65 chronology pairs within a range of 50 km (Figure S2(a)). This association remains significant for up to 1500 km with a mean correlation coefficient of $r = 0.38$ ($p < 0.001$) despite the decreasing number of correlation pairs (average $n = 15$). Inter-species correlation results are similar to those for the same species despite higher replication levels

Table 1. Characteristics of the newly developed composite TRW chronologies with combinations including the number of series per chronology, the start year, the robust period (EPS > 0.85) until the end year, the total length in years, the inter-series correlation (Rbar), the mean sensitivity, and the mean segment length (MSL). Respective species composition can be seen in Figure 3.

| Comp. TRW chronology	Number of series	Start year	EPS > 0.85	End year	Length	Rbar (raw)	Mean sensivity	MSL
Mediterranean	2168	617	1345	2008	1392	0.28	0.22	241
West	1271	924	1330	2008	1085	0.34	0.22	217
West without Italy	1167	924	1305	2008	1085	0.37	0.22	210
East	915	617	1295	2008	1392	0.39	0.22	276
Central Spain	474	1485	1590	2008	524	0.41	0.24	230
Pyrenees	693	924	1330	2007	1084	0.48	0.19	196
Italy	104	1441	1525	2003	563	0.57	0.22	291
Pyrenees plus Italy	797	924	1330	2007	1084	0.42	0.20	208
Balkan	493	617	1295	2008	1392	0.48	0.21	312
Turkey plus Cyprus	422	1379	1555	2004	626	0.45	0.24	234
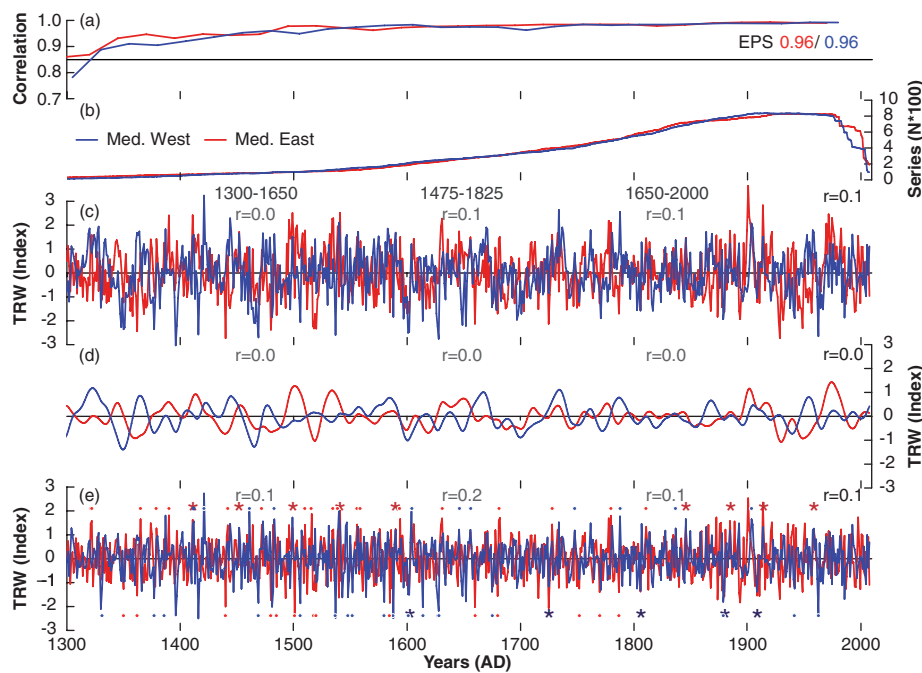
Figure 4. (a) Expressed population signal (EPS) and (b) replication for the (c) PT 150 year SPL detrended and the 20-year (d) low-pass and (e) high-pass filtered composite chronologies West (blue line) and East (red line) with individual (West: blue points; East: red points) and common (asterisks) extreme years. Correlations between West and East were obtained for 338/339-year time windows in grey, and in black for the robust period 1330–2008.

(Figure S2(b)). The highest positive correlation found is $r = 0.41$ in the first 50 km with a replication of 38 chronology pairs. Between 1700 and 3400 km, the correlation coefficients settle around zero increasing slightly afterwards. The correlation decay length for both the inter- and intra-species results can be expressed using a second-degree polynomial fit, with higher explained variance for the intra-species assembly ($R^2 = 0.56$, $p < 0.01$) than for the inter-species one ($R^2 = 0.23$, $p < 0.05$).

The corresponding climate data offer 930 correlation combinations over the period 1901–1976 for temperature means and precipitation sums, and 870 for scPDSI indices, for the winter (DJF) and summer (JJA) season (Figure S3). The DJF and JJA temperatures (Figure S3(a) and (b)) remained positively correlated over a longer distance and appeared more homogeneous ($R^2 = 0.96$–0.97) than

precipitation for the same two seasons ($R^2 = 0.62$–0.66) (Figure S3(c) and (d)). Correlations between DJF temperatures are highly significant ($p < 0.001$) up to 2600 km and JJA temperatures up to 1500 km. Correlation coefficients for precipitation sums for DJF and JJA exceed the 99.9% significance level up to the 600- and 350-km range, respectively. The scPDSI correlations display similar patterns as found with precipitation (Figure S3(e) and (f)).

3.3. Growth–climate responses

The growth–climate response for the Med. chronology (PC1) shows significant negative correlations to summer temperature (May to September: $r = -0.31$, $p < 0.01$) and maximum positive correlations to June/July precipitation with $r = 0.4$ ($p < 0.01$) (Figure 5). Correlations with
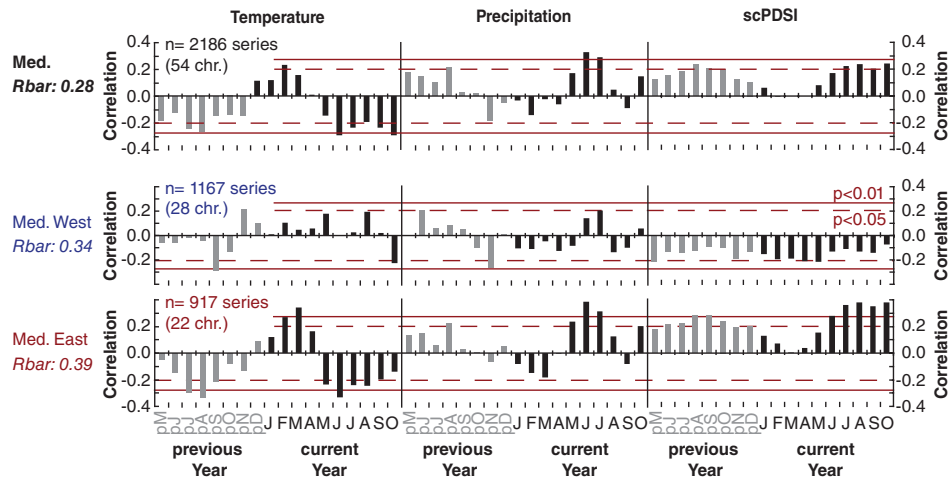
Figure 5. Growth–climate response pattern between PT 150 year SPL detrended Med., Med. West and Med. East composite chronologies and averaged gridded temperature, precipitation, and drought data (CRU TS3.1) calculated over the period 1901–2002 using the 18-month window. Raw Rbar values are shown for each PC subset over their full length and red (dashed) lines indicate the (95%) 99% significance level.
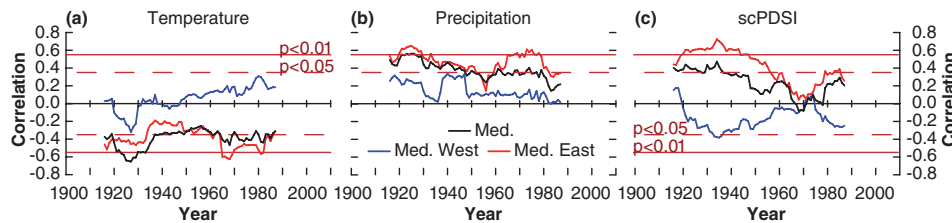

Figure 6. 31-year running correlation of JJA (a) temperature, (b) precipitation, and (c) scPDSI gidded data (CRU TS3.1) against composite TRW-chronology Med. (black), Med. West (blue), and Med. East (red) over the period 1901–2002. Red (dashed) lines indicate the (95%) 99% significance level.

scPDSI were highest for July to September ($r = 0.23$; $p < 0.05$).

The climatic response of the Med. West and Med. East composite TRW chronologies differs strongly. The Med. West shows a generally weaker climate response than Med. East on both spatial and temporal scales (Figures 6 and 7). Med. East correlates positively with scPDSI (from June with $r = 0.28$ up to $r = 0.38$ for October, $p < 0.01$), whereas scPDSI correlations for Med. West are negative (June–October: $r = -0.12$, insignificant). Moreover, the seasonality of the climate response to scPDSI differs between the regions: summer (JJA: $r = 0.35$, $p < 0.01$) for Med. East *versus* spring (MAM: $r = -0.21$, $p < 0.05$) for Med. West. The distinct drought signal in the eastern TRW chronologies is supported by positive correlations with summer (JJA) precipitation ($r = 0.43$, $p < 0.01$) and negative correlations with summer temperatures ($r = -0.34$, $p < 0.01$). Although the growth response to JJA precipitation totals is significant over the entire 20th century, there is a decrease in the growth–climate relationship that occurred during the mid-1950s (Figure 6(b)).

Correlations between precipitation and temperature, and the western chronologies were rarely significant (Figures 5 and 6). JJA temperatures produced strong negative correlations for Med. and Med. E in the eastern Mediterranean Basin, with extension towards Greenland, whereas Med. W shows positive correlations across northern Spain

and the Pyrenees stretching towards west – and central Europe (Figure 7(a)).

Subgroups Med. W1 (central Spain) and Med. W2 (Pyrenees) reveal statistically insignificant growth–climate response patterns for precipitation, and only Med. W2 shows a significantly positive association with temperature in May ($r = 0.28$; $p < 0.05$). Both subgroups yield significant negative correlations to scPDSI in the spring and summer season (April–July: $r = -0.22$, $p < 0.05$). This can be explained by favoured tree growth under warm spring and summer conditions, especially for Med. W2 (Figure S4).

Italy forms a separate cluster based on the first PCA (Figure 3(a)); its correlation results correspond to those for the western Mediterranean. Most notable are the significant negative correlations with spring and summer scPDSI, reaching a maximum in April ($r = -0.24$, $p < 0.05$) (Figure S4). Spatial field correlations for the JJA season, however, show significant ($p < 0.05$) positive associations with JJA temperature across the broader Mediterranean Basin and Europe (Figure S5).

Composite TRW chronologies Med. E1 (Turkey and Cyprus) and Med. E2 (southern Balkans) show negative associations with summer temperatures of the previous as well as the current year, and positive associations with precipitation over the same time period (Figure S4). The strongest correlations for Med. E1 were found with
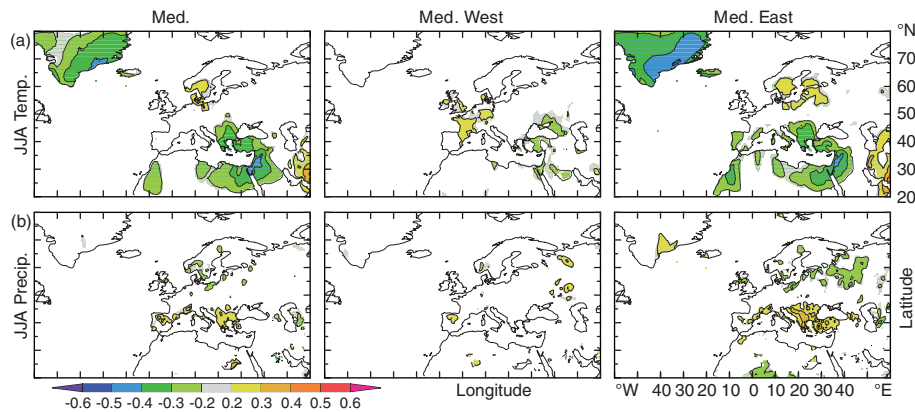
Figure 7. Spatial field correlations for composite TRW chronologies Med. (left), Med. W (centre), and Med. E. (right) against JJA (a) temperature (CRU TS3.1) and (b) precipitation (CRU TS3.1) for the period 1901–2002.

precipitation in May–August ($r = 0.44$, $p < 0.01$). Conditions limiting tree growth are thus found during hot and dry summers (May–August), represented by positive but weak correlations with scPDSI that increase with decreasing latitude from $r = 0.11$ ($p > 0.1$) for Med. E2 to $r = 0.29$ for Med. E1 ($p < 0.01$). Spatial correlations for the JJA season are strongly significant for both subgroups in the eastern Mediterranean and extend towards the south-eastern tip of Greenland, a pattern more distinct for Med. E1 than for Med. E2 (Figure S5).

Overall, our results show that tree growth is controlled by a combination of temperature and precipitation variations in summer, expressed as a dipole growth response between the western and eastern Mediterranean. These differences are also visible at the composite TRW chronology level and at different frequencies (Figure 4).

4. Discussion

4.1. Temporal and spatial variability within the network

We found the first PC axis of a Mediterranean TRW network explains close to 20% of the variance, indicating the existence of a common growth pattern across the Mediterranean. At lower hierarchical orders, the PCA yielded a strict division between the eastern and western Mediterranean, but the position of the central Mediterranean, represented by Italy, remains unclear. Our results show a time-stable discrepancy between West and East Mediterranean sites over the last 700 years (1330–2008) at different temporal resolutions (Figure 4), manifest in the very low number of common extreme years. The majority of positive extreme years, common to both Med. W and Med. E, can be related to volcanic eruptions (i.e. 1450 ± 10 Kuwae, 1580 ± 30 Billy Mitchell, 1845 Hekla, 1883 Krakatau, 1914 Sakurajima; Zielinski, 1995; Oppenheimer, 2003), which cause cooler climate over Europe (Esper *et al.*, 2013) and favourable growing conditions in the Mediterranean Basin.

Significant intra- and inter-species associations between TRW chronologies are largely restricted to a 500-km range (Figure S2). Nevertheless, we found potential connections

over longer distances between a variety of pine species, e.g. *P. heldreichii* and *P. nigra*. In general, the intra-species associations were stronger with some stretching as far as 1500 km. Frank and Esper (2005) found a similar result for a multi-species TRW network in the Alps, as have Kuniholm and Striker (1987) for the Aegean. In the western Mediterranean, Rolland (2002) found strong correlations between remote (>500 km) *P. uncinata* stands, and Richter *et al.* (1991) found similar correlations between four pine species up to 450 km distance.

Mediterranean pine growth associations thus appear to mimic decreasing climatic association trends with increasing distance (Figure S3). Inter-annual temperature variability shows strong homogeneity within a 2500-km radius (e.g. Jones *et al.*, 1997; Büntgen *et al.*, 2010b), but precipitation and summer drought patterns are more regional, due to topography and continentality, and show weaker connections beyond 500 km. It is worth noting that our analyses were based on grid-point data (CRU TS3.1) intended to overcome the absence of long instrumental station data for some regions. These data do not necessarily represent local site conditions, particularly for mountain environments, because the meteorological stations used to produce any given grid-point interpolation are not local to that grid point.

4.2. Climate sensitivity

The comparison of the east and the west pine sites shows a minor elevational bias (Figure 8(d)), but elevation does not play a crucial role in the climate signal of the pine composite chronologies (Table S1 and Figure S4). We found that pine growth at mid- and high altitudes (1500–2250 m a.s.l.) has a drought or a mixed climate signal, whereas pines at the maximum elevation tree-line sites in the Pyrenees (2250–2500 m a.s.l.) primarily respond to late spring–summer temperature (Table S1 and Figure S4). It is important to note that we focused our analysis on strong climate signals in mid-to-high elevation pines and thus have not considered the climate response of pine sites below 1500 m a.s.l. in our analyses.

The Mediterranean TRW network is divided into biogeographically coherent subregions despite lacking an
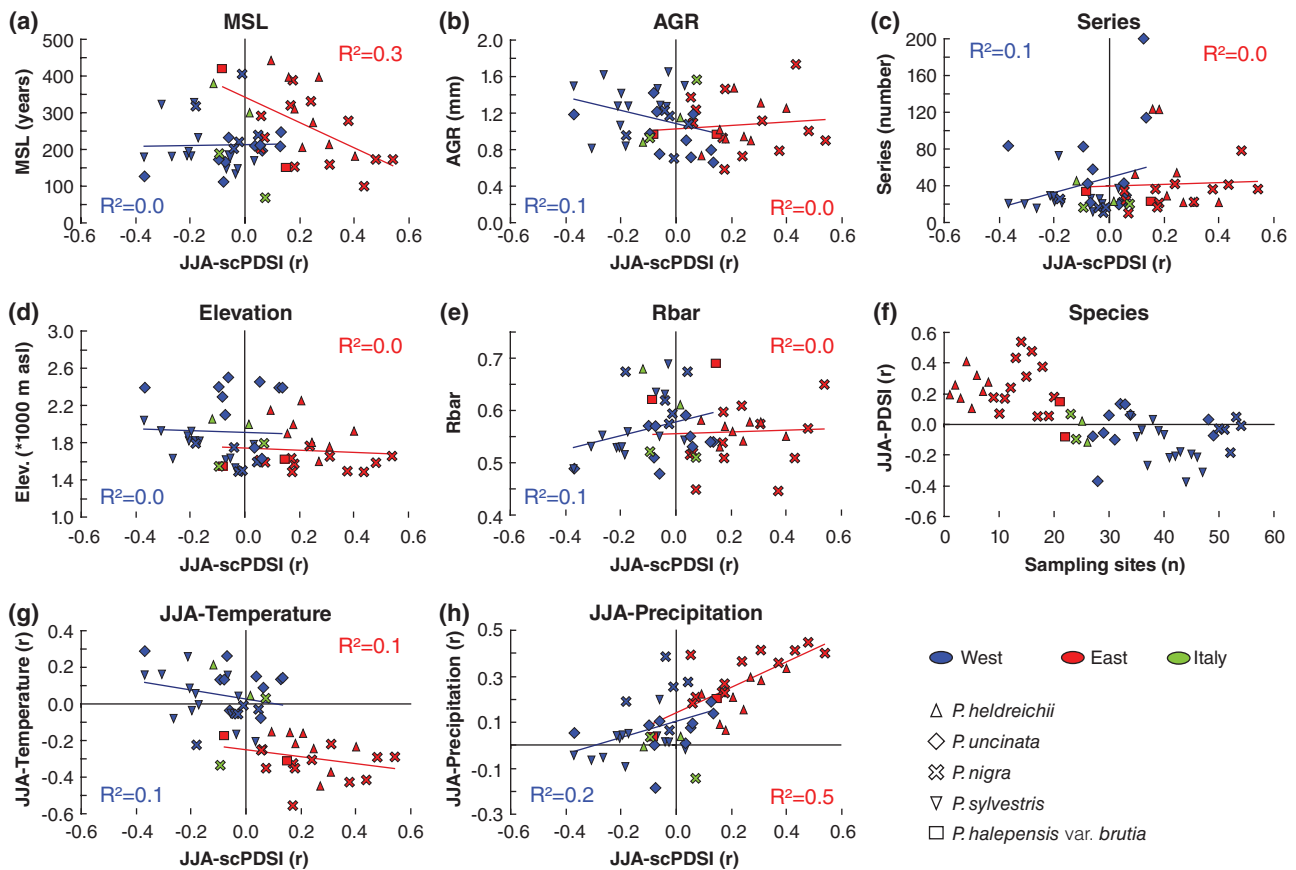
Figure 8. JJA-scPDSI grid-point correlations of each site computed against its respective (a) mean segment length (MSL), (b) average growth rate (AGR), (c) number of series, (d) elevation, (e) inter-series correlation, (f) species, (g) JJA-temperature means, and (h) JJA-precipitation sums. R^2 describes the trend of a linear regression model. Please note changes in scales and inverse axes in (f).

evenly distributed network of sampling sites. This implies that environmental factors, rather than species-specific influences, dominate tree growth (Figure 8). For instance, *Pinus nigra*, present in the eastern and western Mediterranean, shows a contrasting response to summer drought which depresses tree growth in the western Mediterranean, but promotes it in the East (Figure 8(f)). In general, trees in the western Mediterranean share a stronger common signal (explained common variance of 29.5%), but the growth–climate response is more moderate than for the eastern Mediterranean. The stronger common signal in the western pine chronologies can be explained by the smaller geographical range covered by those sites. The low climate sensitivity may be explained by ecological controls on growth: cooler temperatures at high elevations enhance temperature limitations on tree growth (e.g. in the Pyrenees) in addition to drought influences, leading to a mixed climatic response. In contrast, maximum latewood density measurements for high elevation pines in the Pyrenees contain a univocal warm season temperature signal (Büntgen *et al.*, 2010a). Evaporative demand and precipitation are generally lower at lower elevations, whereas radial growth in dry regions is predominantly constrained by drought (e.g. in central Spain) (Figure S4).

The western pines thus react negatively to drought and their growth–climate response pattern resembles that

identified by Richter *et al.* (1991). These results are in accordance with earlier studies for the Pyrenees where positive but weak and unstable correlations to summer temperatures were found (Tardif *et al.*, 2003; Büntgen *et al.*, 2010a). A higher diversity of growth–climate relations was found for central Spain. Gutiérrez (1989) stated that drought at the beginning of the growing season (March) and in summer (June) affect *P. sylvestris* growth in southern Catalonia. *P. uncinata* from the central plains of Spain (Genova, 1986) and *P. nigra* from the eastern part of the Iberian Peninsula (Martín-Benito *et al.*, 2010) show a summer drought signal that is further enhanced in Southern Spain (Richter *et al.*, 1991).

Summer drought is also the strongest climate signal in TRW records of the eastern Mediterranean region. The strength of the drought signal generally increases with decreasing latitude and increasing eastern longitude from the Balkans (Med. E2) to Turkey and Cyprus (Med. E1). A rather weak and unstable climate signal was observed in some regional studies, especially for *P. heldreichii* at high elevation sites in the Balkan region (Panayotov *et al.*, 2010; Seim *et al.*, 2012). Further south, where the Mediterranean climate is more pronounced (Figure 1(b)), a strong positive influence of summer precipitation has resulted in numerous drought reconstructions derived from a variety of pine species (e.g. D'Arrigo and Cullen, 2001; Touchan

et al., 2003; Akkemik and Aras, 2005), and confirms the higher potential for TRW-based drought reconstructions using pines in the eastern rather than the western Mediterranean region. Touchan *et al.* (2014) even identified subregional patterns and the high potential for seasonal climate reconstructions in a multi-species network study for the eastern Mediterranean.

A potential reason for the seasonal shift in climate response is the development of different strategies to compensate for dehydration. Pines in Med. West need to adapt to drought conditions at the beginning of the growing season (spring/early summer), whereas pines in Med. East are generally more stressed during summer (Figure 5). Evidence for structural adaption to drought is provided in a study of *P. sylvestris* along a north–south transect across Europe by Palmroth *et al.* (1999) and Martinez-Vilalta *et al.* (2009). Especially at mountain sites where shallow soils have a limited water storage capacity, water deficit during hot summers causes (1) changes in the cell structure by increasing the cell lumen diameter to improve water conduction (Eilmann *et al.*, 2011) and (2) a general reduction in cell number leading to narrower tree rings especially at high altitudes (e.g. Gruber *et al.*, 2010).

4.3. Climate dynamic effects on mountain pine tree growth

The identified groupings of the pine TRW network can only be explained by differences in synoptic climate pattern across the Mediterranean. Mediterranean pine growth is mainly influenced by synoptic-scale patterns of summer drought, which is consistent with the first canonical mode of summer temperature data (1950–1999) across the Mediterranean region found by Xoplaki *et al.* (2003). During summer, insolation is increased, due to predominantly clear skies, and a stable warm high pressure in the Mediterranean Basin (Xoplaki *et al.*, 2003).

Additionally, the second canonical mode found by Xoplaki *et al.* (2003) highlights differences in climate between the western and the eastern Mediterranean, which supports the poor agreement between the composite chronologies Med. East and Med. West (Figures 4 and 7). One reason for the east–west difference in summer climate lies in the influence of the East Atlantic jet stream expressed by westerly winds, which have a stronger cooling effect in the West compared with the East (Dünkeloh and Jacobeit, 2003; Xoplaki *et al.*, 2003). Moreover, both empirical and ensemble modelling evidence, based on an array of climate variables, identified variability in the western Mediterranean that co-varies with the West African Monsoon (Fontaine *et al.*, 2010). Finally, the summer North Atlantic Oscillation (sNAO) is a strong driver of temperature variability in the eastern Mediterranean, but not in the West (Folland *et al.*, 2009; Trouet *et al.*, 2012).

In addition to this, the oceanic-continental gradient ranging from Spain to Turkey is interrupted by the Mediterranean Sea, a pool of permanent heat and vapour exchange, and by regional winds such as the Westerly, Mistral, and Sirocco. This leads to a complex Mediterranean climate with multiple drivers, especially in summer

(Pauling *et al.*, 2006). Further reasons for spatial climate differences can be found in Hadley circulation that triggers the overturning of air masses in the troposphere and shows a descending motion in the subtropics (Hadley, 1735). This circulation is strongly related to west–east jet streams (tropopause-level westerlies) and varies seasonally (Dima and Wallace, 2003). In summer, the Hadley cell moves northwards, towards eastern North Africa, and the impact of the Asian monsoon in the mid-troposphere becomes stronger, particularly in the eastern Mediterranean (Ziv *et al.*, 2004). According to Ziv *et al.* (2004), the Asian monsoon enhances the subsidence of air masses over the east Mediterranean and enforces the Etesian winds equalizing low-level pressure differences between the two regions. The prevailing low-pressure system across the eastern Mediterranean is linked with high-pressure areas in Northwest, East but also in Central Europe (Arseni-Papadimitriou *et al.*, 1988; Luterbacher *et al.*, 2012). These linkages are confirmed by Ziv *et al.* (2004) for the sNAO, the leading eigenvector for July/August mean sea level pressure over the North Atlantic (Hurrell and Folland, 2002). Proxy evidence (1768–2008) for a teleconnection pattern between the Balkans and north-western Europe was found by Trouet *et al.* (2012), who developed a temperature reconstruction for Bulgaria (Balkan, eastern Mediterranean) using tree-ring maximum latewood density.

5. Conclusion

A Mediterranean pine network of 2186 individual TRW measurement series from 54 mid- to high-elevation sites was compiled and analysed. The first PCA contains almost 20% of the total network variance, whereas higher-order components demonstrate that tree-ring variability differs significantly between the West and East Mediterranean regions. The east–west dipole in pine growth is supported by the correlation decay of ∼500 km representing decreasing drought association trends with increasing distance. The climate–growth response of pines in the western part of the network is more moderate favouring warm temperatures in spring and early summer, especially in the Pyrenees, probably caused by site characteristics. By contrast, the growth rates of pines in the East are higher under cold-wet conditions. Specific atmospheric circulation patterns and corresponding differences in climatic drivers likely cause the distinct, zonal, inter-annual to decadal-scale growth response patterns. Our results point to a larger potential for TRW-based drought reconstructions in the eastern Mediterranean region as opposed to the West, but demonstrate in general the challenges for climate reconstructions based on mid- to high-elevation Mediterranean pines.

Supporting Information

The following supporting information is available as part of the online article:

Table S1. Characteristics of the site chronologies including species (PIBR = *P. halepensis* var. *brutia*, PIHE = *P. heldreichii*, PILE = *P. heldreichii* var. *leucodermis*, PINI = *P. nigra*, PISY = *P. sylvestris*, PIUN = *P. mugo* spp. *uncinata*), latitude (°N), longitude (°E), elevation (m a.s.l.), covered period (AD), number of series, mean segment length (MSL), average growth rates (AGR), inter-series correlation (Rbar), contributor (data derived from the ITRDB are indicated by a hash sign), Pearson correlation with June–August temperatures and precipitation amounts, respectively, for the period 1901–2002 AD. Correlation values exceeding the 95% (99%) significance level are denoted with one (two) star(s).

Figure S1. Dendrogram using average linkage between groups (Pearson correlation) for the period 1862–1976 AD. Colors used for the species correspond to Figure 1 except for *Pinus sylvestris* (PISY).

Figure S2. Individual correlations (grey points and triangles) and their averages over 100 km distance classes lagged by 50 km (black points and triangles) and the corresponding replication (black lines) for (a) within species (grey triangles) and (b) between species (grey circles). Red dashed lines indicate the 99.9% significance level and R^2 describes the explained variance of a second degree polynomial regression model.

Figure S3. Individual correlations (grey points) and their averages over 100 km distance classes lagged by 50 km (black points) and the corresponding replication (black lines) for (a) DJF and (b) JJA temperature means, (c) DJF and (d) JJA precipitation amounts, and (e) DJF and (f) JJA scPDSI values (CRU TS3.1). Red dashed lines indicate the 99.9% significance level and R^2 describes the explained variance of a second-degree polynomial regression model.

Figure S4. Growth–climate response patterns between PT 150 year spline detrended subgroup chronologies and averaged gridded temperature, precipitation and drought data (CRU TS3.1) calculated over the period 1901–2002 using the 18-month window. Raw Rbar values are shown for each PC subset and red (dashed) lines indicate the (95%) 99% significance level.

Figure S5. Spatial field correlations of subgroup composite TRW chronologies against JJA temperature (left) and precipitation (right; CRU TS3.1) for the period 1901–2002.

References

Akkemik Ü, Aras A. 2005. Reconstruction (1689–1994 AD) of April–August precipitation in the southern part of central Turkey. *Int. J. Climatol.* **25**: 537–548.

Arseni-Papadimitriou A, Maheras P, Giles BD. 1988. Contribution to the study of the strong north winds on Aegean Sea, in the warm season. *Riv. Meteorol. Aeronaut.* **48**(3-4): 131–138.

Barbéro M, Loisel R, Quézel P, Richardson DM, Romane F. 1998. Pines of the Mediterranean Basin. In *Ecology and Biogeography of Pinus*, Richardson DM (ed). Cambridge University Press: Cambridge, UK, 153–170.

Büntgen U, Frank D, Trouet V, Esper J. 2010a. Diverse climate sensitivity of Mediterranean tree-ring width and density. *Trees* **24**: 261–273.

Büntgen U, Franke J, Frank D, Wilson R, González-Rouco F, Esper J. 2010b. Assessing the spatial signature of European climate reconstructions. *Clim. Res.* **41**: 125–130.

Cook ER, Krusic PJ. 2010. *Software*. Tree Ring Laboratory of Lamont-Doherty Earth Observatory. http://www.ldeo.columbia.edu/tree-ring-laboratory/resources/software (accessed 25 June 2010).

Cook ER, Peters K. 1997. Calculating unbiased tree-ring indices for the study of climatic and environmental change. *Holocene* **7**: 361–370.

D'Arrigo RD, Cullen HM. 2001. A 350-year (AD 1628–1980) reconstruction of Turkish precipitation. *Dendrochronologia* **19**: 167–177.

Dima IM, Wallace JM. 2003. On the seasonality of the Hadley cell. *J. Atmos. Sci.* **60**: 1522–1527.

Dünkeloh A, Jacobeit J. 2003. Circulation dynamics of Mediterranean precipitation variability 1948–98. *Int. J. Climatol.* **23**(15): 1843–1866.

Eilmann B, Zweifel R, Buchmann N, Graf Pannatier E, Rigling A. 2011. Drought alters timing, quantity, and quality of wood formation in Scots pine. *J. Exp. Bot.* **62**(8): 2763–2771.

Esper J, Schneider L, Krusic PJ, Luterbacher J, Büntgen U, Timonen M, Sirocko F, Zorita E. 2013. European summer temperature response to annually dated volcanic eruptions over the past nine centuries. *Bull. Volcanol.* **75**: 736, doi: 10.1007/s00445-013-0736-z.

Folland CK, Knight J, Linderholm HW, Fereday D, Ineson S, Hurrell JW. 2009. The summer North Atlantic Oscillation: past, present, and future. *J. Clim.* **22**: 1082–1103.

Fontaine B, Garcia-Serrano J, Roucou P, Rodriguez-Fonseca B, Losada T, Chauvin F, Gervois S, Sijikumar S, Ruti P, Janicot S. 2010. Impacts of warm and cold situations in the Mediterranean basins on the West African monsoon: observed connection patterns (1979–2006) and climate simulations. *Clim. Dyn.* **35**: 95–114.

Frank DC, Esper J. 2005. Characterization and climate response patterns of a high-elevation, multi-species tree-ring network in the European Alps. *Dendrochronologia* **22**: 107–121.

Gao X, Giorgi F. 2008. Increased aridity in the Mediterranean region under greenhouse gas forcing estimated from high resolution simulations with a regional climate model. *Glob. Planet. Change* **62**: 195–209.

Genova R. 1986. Dendroclimatology of mountain pine (*Pinus uncinata* Ram.) in the central plain of Spain. *Tree-Ring Bull.* **46**: 3–12.

Grissino-Mayer HD, Fritts HC. 1997. The International Tree-Ring Data Bank: an enhanced global database serving the global scientific community. *Holocene* **7**: 235–238.

Gruber A, Strobl S, Veit B, Oberhuber W. 2010. Impact of drought on the temporal dynamics of wood formation in *Pinus sylvestris*. *Tree Physiol.* **30**(4): 490–501.

Gutiérrez E. 1989. Dendroclimatological study of *Pinus sylvestris* L. in southern Catalonia (Spain). *Tree-Ring Bull.* **49**: 1–9.

Hadley G. 1735. Concerning the cause of the general trade-winds. *Philos. Trans.* **29**: 58–62.

Holmes RL. 1983. Computer assisted quality control in tree-ring dating and measurement. *Tree-Ring Bull.* **43**: 69–78.

Hughes MK, Kuniholm PI, Eischeid JK, Garfin G, Griggs CB, Latini C. 2001. Aegean tree-ring signature years explained. *Tree-Ring Res.* **57**(1): 67–73.

Hurrell JW, Folland CK. 2002. The relationship between tropical Atlantic rainfall and the summer circulation over the North Atlantic. *CLIVAR Exchanges* **25**: 52–54.

IPCC. 2013. *Climate Change 2013: The Physical Science Basis. Contribution of Working Group I to the Fifth Assessment Report of the Intergovernmental Panel on Climate Change*. Cambridge University Press: Cambridge, UK and New York, NY.

Jones PD, Osborn TJ, Briffa KR. 1997. Estimating sampling errors in large-scale temperature averages. *J. Clim.* **10**: 2548–2568.

Kuniholm PI, Striker CL. 1987. Dendrochronological investigations in the Aegean and neighboring regions, 1983–1986. *J. Field Archaeol.* **14**(4): 385–398.

Ludwig JA, Reynolds JF. 1988. *Statistical Ecology*. John Wiley & Sons: New York, NY.

de Luis M, Čufar K, Di Filippo A, Novak K, Papadopoulos A, Piovesan G, Rathgeber CBK, Raventós J, Angel Saz M, Smith KT. 2013. Plasticity in dendroclimatic response across the distribution range of Aleppo pine (*Pinus halepensis*). *PLoS One* **8**(12): e83550, doi: 10.1371/journal.pone.0083550.

Luterbacher J, García-Herrera R, Akcer-On S, Allan R, Alvarez-Castro MC, Benito G, Booth J, Büntgen U, Cagatay N, Colombaroli D, Davis B, Esper J, Felis T, Fleitmann D, Frank D, Gallego D, Garcia-Bustamante E, Glaser R, González-Rouco JF, Goosse H, Kiefer T, Macklin MG, Manning SW, Montagna P, Newman L, Power MJ, Rath V, Ribera P, Riemann D, Roberts N, Silenzi S, Tinner W, Valero-Garces B, van der Schrier G, Tzedakis C, Vannière B, Vogt S, Wanner H, Werner JP, Willett G, Williams MH, Xoplaki E, Zerefos CS, Zorita E. 2012. A review of 2000 years of paleoclimatic evidence in the Mediterranean. In *The Climate of the Mediterranean Region: From the Past to the Future*, Lionello P (ed). Elsevier: Amsterdam, 87–185.

Martín-Benito D, del Río M, Cañellas I. 2010. Black pine (*Pinus nigra* Arn.) growth divergence along a latitudinal gradient in Western Mediterranean mountains. *Ann. For. Sci.* **67**(4): 401, doi: 10.1051/forest/2009121.

Martinez-Vilalta J, Cochard H, Mencuccini M, Sterck F, Herrero A, Korhonen JFJ, Llorens P, Nikinmaa E, Nolè A, Poyatos R, Ripullone F, Sass-Klaassen U, Zweifel R. 2009. Hydraulic adjustment of Scots pine across Europe. *New Phytol.* **184**(2): 353–364.

Mitchell TD, Jones PD. 2005. An improved method of constructing a database of monthly climate observations and associated high-resolution grids. *Int. J. Climatol.* **25**: 693–712.

Nicault A, Alleaume S, Brewer S, Carrer M, Nola P, Guiot J. 2008. Mediterranean drought fluctuations during the last 500 years based on tree-ring data. *Clim. Dyn.* **31**: 227–245.

van Oldenborgh GJ, Burgers G. 2005. Searching for decadal variations in ENSO precipitation teleconnections. *Geophys. Res. Lett.* **32**(15): L15701, doi: 10.1029/2005GL023110.

Oppenheimer C. 2003. Ice core and palaeoclimatic evidence for the timing and nature of the great mid-13th century volcanic eruptions. *Int. J. Climatol.* **23**: 417–426.

Palmroth S, Berninger F, Nikinmaa E, Lloyd J, Pulkkinen P, Hari P. 1999. Structural adaptation rather than water conservation was observed in Scots pine over a range of wet and dry climates. *Oecologia* **121**: 302–309.

Panayotov M, Bebi P, Trouet V, Yurukov S. 2010. Climate signals in *Pinus peuce* and *Pinus heldreichii* tree-ring chronologies from the Pirin Mountains in Bulgaria. *Trees* **24**: 479–490.

Pauling A, Luterbacher J, Casty C, Wanner H. 2006. Five hundred years of gridded high-resolution precipitation reconstructions over Europe and the connection to large-scale circulation. *Clim. Dyn.* **26**: 387–405.

Peters K, Jacoby GC, Cook ER. 1981. Principal components analysis of tree-ring sites. *Tree-Ring Bull.* **41**: 1–19.

Richter K, Eckstein D, Holmes RL. 1991. The dendrochronological signal of pine trees (*Pinus* spp.) in Spain. *Tree-Ring Bull.* **51**: 1–13.

Rolland C. 2002. Decreasing teleconnections with inter-site distance in monthly climatic data and tree-ring width networks in a mountainous Alpine area. *Theor. Appl. Climatol.* **71**: 63–75.

van der Schrier G, Briffa KR, Jones PD, Osborn TJ. 2006. Summer moisture variability across Europe. *Int. J. Climatol.* **19**: 2818–2834.

Seim A, Büntgen U, Fonti P, Haska H, Herzig F, Tegel W, Trouet V, Treydte K. 2012. Climate sensitivity of a millennium-long pine chronology from Albania. *Clim. Res.* **51**: 217–228.

Sousa PM, Trigo RM, Aizpurua P, Nieto R, Gimeno L, Garcia-Herrera R. 2011. Trends and extremes of drought indices throughout the 20th century in the Mediterranean. *Nat. Hazards Earth Syst. Sci.* **11**: 33–51.

Tardif J, Camarero JJ, Ribas M, Gutiérrez E. 2003. Spatiotemporal variability in tree growth in the Central Pyrenees: climatic and site influences. *Ecol. Monogr.* **73**(2): 241–257.

Touchan R, Garfin G, Meko DM, Funkhouser G, Erkan N, Hughes MK, Wallin BS. 2003. Preliminary reconstructions of spring precipitation in Southwestern Turkey from tree-ring width. *Int. J. Climatol.* **23**: 157–171.

Touchan R, Anchukaitis KJ, Shishov VV, Sivrikaya F, Attieh J, Ketmen M, Stephan J, Mitsopoulos I, Christou A, Meko DM. 2014. Spatial patterns of eastern Mediterranean climate influence on tree growth. *Holocene* **24**(4): 381–392, doi: 10.1177/0959683613518594.

Trouet V, van Oldenborgh GJ. 2013. KNMI Climate Explorer: a web-based research tool for high-resolution paleoclimatology. *Tree-Ring Res.* **69**(1): 3–13.

Trouet V, Panayotov MP, Ivanova A, Frank DC. 2012. A pan-European summer teleconnection mode revealed by a new temperature reconstruction from the northeastern Mediterranean (1768–2008). *Holocene* **22**(8): 887–898, doi: 10.1177/0959683611434225.

Wigley TML, Briffa KR, Jones PD. 1984. On the average of correlated time series, with applications in dendroclimatology and hydrometeorology. *J. Clim. Appl. Meteorol.* **23**: 201–213.

Xoplaki E, Gonzalez-Rouco JF, Luterbacher J, Wanner H. 2003. Mediterranean summer air temperature variability and its connection to the large-scale atmospheric circulation and SSTs. *Clim. Dyn.* **20**: 723–739.

Zielinski GA. 1995. Stratospheric loading and optical depth estimates of explosive volcanism over the last 2100 years derived from the Greenland Ice Sheet Project 2 ice core. *J. Geophys. Res.* **100**(D10): 20937–20955.

Ziv B, Saaroni H, Alpert P. 2004. The factors governing the summer regime of the eastern Mediterranean. *Int. J. Climatol.* **24**: 1859–1871.